Accepted to Optics Express, 2019

First experimental realization of six-pack holography and its application to dynamic synthetic aperture superresolution

SIMCHA K. MIRSKY AND NATAN T. SHAKED*

Department of Biomedical Engineering, Faculty of Engineering, Tel Aviv University, Tel Aviv 69978, Israel

*nshaked@tau.ac.il

Abstract: It has long been assumed that off-axis holography is less spatial bandwidth efficient than on-axis holography. Six-pack holography (6PH) is the first off-axis configuration that changes this paradigm. We present the first experimental realization of 6PH, an off-axis interferometric system capable of spatially multiplexing six complex wavefronts while using the same number of camera pixels needed for a single off-axis hologram. Each of the six parallel complex wavefronts is encoded using a different fringe orientation and can be fully reconstructed. This technique is especially useful for dynamic samples, as it allows the acquisition of six complex wavefronts simultaneously. There are many applications for the data that can be compressed into the six channels. Here, we utilize 6PH to increase resolution in dynamic synthetic aperture imaging, where each of the six optically compressed off-axis holograms encodes a different spatial frequency range of the imaged sample, yielding 1.62× resolution enhancement.

1. Introduction

Holography can record the entire complex wavefront (amplitude and phase) of the light interacting with the sample by recording interference between a beam that has interacted with the sample and a reference beam that does not contain the sample spatial modulation. There are two main approaches to holographic wavefront acquisition: on-axis and off-axis holography. In on-axis holography [1], the two beams interfere with no angle between them, which causes mixing of the sample and reference intensities with the complex wavefront of the sample. For a non-sparse sample, this approach requires the acquisition of three or four phase-shifted holograms of the same sample instance in order to isolate the sample's complex wavefront from the undesired complex wave data. If these holograms are acquired sequentially, i.e. at different times, fast dynamic processes cannot be recorded. However, in order to acquire the holograms simultaneously, three or four camera planes are needed, requiring extended sensor sizes with slower frame rates and resulting in registration problems between the different camera planes. Off-axis holography [2], on the other hand, captures the complex wavefront of the sample within a single camera exposure. This single-exposure complex wavefront acquisition is accomplished in off-axis holography by inducing a small angle between the sample and reference beams creating the interference pattern of the hologram, and is highly relevant for quantitatively imaging dynamic samples. This single-exposure mode is possible since in the spatial frequency domain, there is a full separation between the auto-correlation term, originating from the sample and reference beam intensities, and the cross-correlation (CC) terms, each of which contains the complex wavefront of the sample. The spatial frequency separation in off-axis holography typically occurs across a single axis, allowing the compression of more information along other axes as well, thereby taking advantage of the unused space in the spatial frequency domain. This can be achieved experimentally by multiplexing several holograms with different interference fringe orientations into a single multiplexed hologram, followed by full reconstruction of the complex wavefronts encoded. Each of these holograms can contain additional data on the imaged sample, meaning that multiplexing enables the acquisition of more information while using the same number of camera pixels. This is beneficial for highly dynamic samples as more dynamic data can be recorded simultaneously.

Various holographic techniques can benefit from the multiplexed parallel data channels, such as extended field of view of imaging [3], multicolor imaging [4], measuring the Jones matrix (and the birefringence) [5], or measuring fluorescence and quantitative phase profiles together [6], tomographic phase microscopy with less angular scanning for 3D refractive index imaging [7], multi-depth imaging [8], and holographic imaging of ultrafast events using laser pulses [9].

In this paper, we experimentally realize a new off-axis multiplexing holographic geometry, named six-pack holography (6PH), which presents, for the first time, an off-axis holography modality that is more camera spatial bandwidth efficient than on-axis holography. 6PH uses partially coherent light and a phase delay plate, and enables simple simultaneous acquisition of six holographic channels, making it attractive for imaging dynamics.

2. Six-pack holography (6PH)

Six-pack holography (6PH) allows the compression of six complex wavefronts into a single multiplexed off-axis hologram without loss of magnification or resolution, where the multiplexed hologram contains straight off-axis fringes of six different orientations. In [10] and [11], we only showed simulation results, in which we took a dynamic hologram of the sample and digitally compressed six successive frames into one multiplexed hologram, and then reconstructed the six complex wavefronts encoded. However, experimental realization of 6PH is not trivial. First, it requires six interference channels, which may make the optical system very complex and not feasible for realization; second, in addition to the desired channels, non-matching sample or reference beams also induce interference terms that typically overlap with useful interference terms in the spatial-frequency domain; third, the camera's grayscale dynamic range is shared by the multiplexed holographic channels. These problems are solved and discussed below.

This paper presents the first experimental realization of 6PH, in which six imaging channels are simultaneously acquired. Being able to perform highly rapid acquisition of complex wavefronts in a quantitative, non-destructive, and nonintrusive manner is expected to open new horizons for biomedical and metrological applications, with focus on the acquisition of quantitative complex wavefronts of highly dynamic processes of transparent and semi-transparent samples, such as flowing biological cells in vitro and lithography/etching processes.

Until now, it has been well known that a single off-axis hologram requires four times more pixels than a single on-axis hologram, whereas on-axis holography requires the acquisition of three phase-shifted holograms in order to reconstruct the complex wavefront. As shown in Fig. 1(a), assuming that a single on-axis hologram requires $N \times N = N^2$ pixels, then one needs $3N^2$ pixels in order to reconstruct the complex wavefront of the sample using on-axis holography. Standard off-axis holography, on the other hand, would require $4N \times 4N = 16N^2$ pixels to acquire the same wavefront, as shown in Fig. 1(b), but would only need a single exposure, making it more suitable for dynamic samples, but consuming more of the camera spatial bandwidth. 6PH compresses six complex wavefronts into the same number of camera pixels. Thus, as shown in Fig. 1(c), in 6PH, $16N^2$ pixels, the same number of pixels used for a single off-axis hologram, are enough to acquire six complex wavefronts, whereas in the case of on-axis holography, we would need $3N^2 \times 6 = 18N^2$ pixels to acquire the same six complex wavefronts. Thus, six-pack off-axis holography is 12.5% more spatial bandwidth efficient than on-axis holography, and at least 50% more bandwidth efficient than other off-axis holography multiplexing methods [12-22].

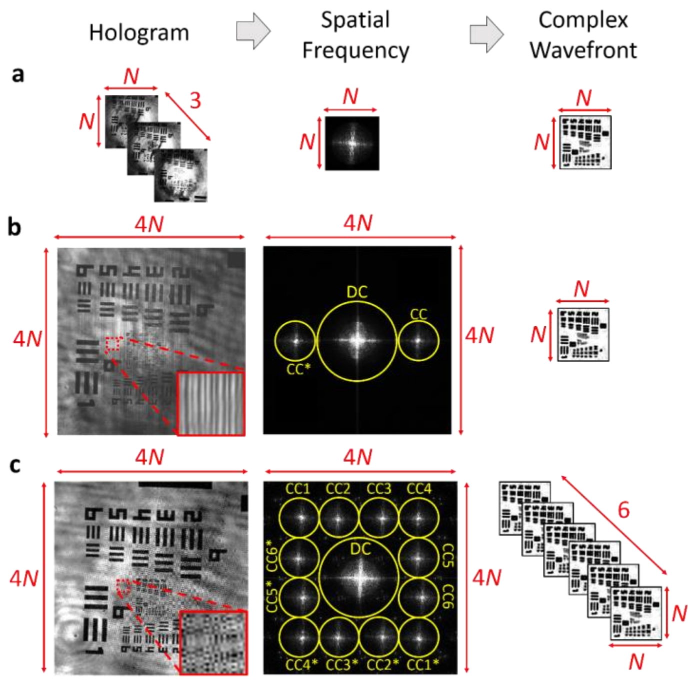

Fig. 1. Comparison of on-axis holography, standard off-axis holography, and 6PH. These holograms were acquired with the experimental system presented next. CC, cross-correlation term; CC*, complex conjugate of corresponding CC term; DC, auto-correlation term. (a) Using on-axis holography, three $N \times N$ on-axis holograms are required to reconstruct a single $N \times N$ complex wavefront (on-axis: $3N^2 \rightarrow N^2 = 18N^2 \rightarrow 6N^2$). (b) Using typical off-axis holography, a single $4N \times 4N$ off-axis hologram is required to reconstruct a single $N \times N$ complex wavefront (off-axis: $16N^2 \rightarrow N^2$). (c) Using 6PH, a single $4N \times 4N$ off-axis multiplexed hologram is required to reconstruct six $N \times N$ complex wavefronts (6PH: $16N^2 \rightarrow 6N^2$). The insets in (b) and (c) show the corresponding fringes magnified ten times.

It should be noted that 6PH assumes the general case in which the sample is not sparse in any spatial dimension, as oppose to other works that allow larger number of multiplexed channels for sparse sample [23]. In this case, 6PH represents the optimal compression ratio for experimentally acquired holograms. Furthermore, 6PH does not have pixel registration problems, as would be the case when acquiring three parallel channels of on-axis holography for capturing fast dynamics. As 6PH projects six holographic channels on the camera simultaneously, it may require cameras with higher grayscale dynamic range, depending on the absorbance properties of the sample.

3. 6PH optical system

We have chosen to demonstrate the first utilization of 6PH for increasing resolution in dynamic holographic imaging using a simultaneous synthetic aperture (SA) superresolution approach [24,25]. In SA superresolution, the sample is illuminated from various angles other than normal incidence, resulting in downshifting the sample spatial frequencies, and enabling the acquisition of higher frequencies that would not normally enter the aperture of the microscope objective. The spatial frequencies of the acquired images can then be stitched to together to create a wider SA containing the higher frequencies that were previously lacking in an image of normal-incidence illumination. Performing an inverse Fourier transform will then produce a superresolved image, which emulates an increased effective numerical aperture (NA). This SA imaging approach can be combined with digital holography for complex wavefront acquisition with increased resolution [26-32].

The multiple images created by illuminating the sample from different angles, which are needed to produce a SA image, can simply be acquired sequentially at different times [26-31], or simultaneously in a single camera exposure by using spatial multiplexing [26,32]. When combined with multiplexed off-axis holography, each of the SA perspective images can be encoded into off-axis holograms of different fringe orientations, and all off-axis holograms can be acquired in a single exposure.

The 6PH system we designed is a modified Mach-Zehnder interferometer, illustrated in Fig. 2(a). In the system, a beam of partially coherent laser light illuminates a diffractive beam shaper DBS producing 77 collimated beams in a diverging 11 × 7 pattern. Figure 2(b) illustrates two of the six beams illuminating the sample from different angles in the sample arm of the interferometer. As shown in this figure, the beams in this pattern alternate between diverging and being parallel to each other as they pass through the lenses. The beams then traverse lens L1 and enter beam splitter BS1.

In the sample arm, the beams then traverse lens L2, periscope P1, and lens L3. Before passing through lens L4 the undesired beams are blocked and the remaining six beams, illustrated in Fig. 2(c), pass through a phase delay plate, PDP, where each beam passes through a different number of glass sections, as illustrated in Fig. 2(c) (see Appendix 1 for full details). This prevents the six sample beams from interfering with each other on the camera. A similar PDP is used in the reference arm, thus solving the problem of undesired interference between the numerous sample and reference beams of the six channels. The six delayed sample beams then pass through L4 and illuminate the sample at six angles. The light scattered by the sample is then collected and imaged on digital camera C by microscope objective MO and lens L5, passing through beam splitter BS2, where the samples beams are combined with their reference pairs.

In the reference arm, nearly the same optical path is experienced by the reference beams. The only significant differences are that six different beams are blocked and a correspondingly different PDP is used, as in Fig. 2(c). These changes, as well as different focal lengths for L8 to L10 compared to L4 and L5, are in order to produce the correct off-axis angles on the camera required for 6PH. Further details on the system can be found in Appendix 1.

Once the six-pack hologram is captured in a single camera exposure, a single digital 2D Fourier transform is performed, and the 6 CC terms corresponding to the six complex wavefronts from the six illumination angles are cropped. The SA is then constructed by positioning the CC terms according to the relative downshift of the frequencies they contained and the direction of illumination.

4. Experimental results

A positive 1951 USAF target was imaged by the system, and a SA was created using the process detailed above. To compensate for beam curvatures, a hologram without the USAF target present (a background image) was also captured, and a background SA was created using the same process. The inverse Fourier transform of the USAF SA was pixel-wise divided by the inverse Fourier transform of the background SA, and the absolute value was taken, thereby generating an amplitude image of the USAF target. The six-pack hologram of the USAF and its 2D Fourier transform are shown in Figs. 3(a) and 3(b), respectively. The SA was created by cropping the six CC terms, repositioning them, and then cropping to the largest possible centered circle with no missing frequencies. The CC term positioning when creating the SA, and the final cropped SA, are shown in Figs. 3(c) and 3(d). The reconstructed amplitude image obtained after performing an inverse Fourier transform is shown in Fig. 3(e). For comparison, the same test target was imaged by the system using a normal-incidence illumination beam and a single reference beam to provide a standard off-axis hologram. These results are shown in shown in Fig. 4(a).

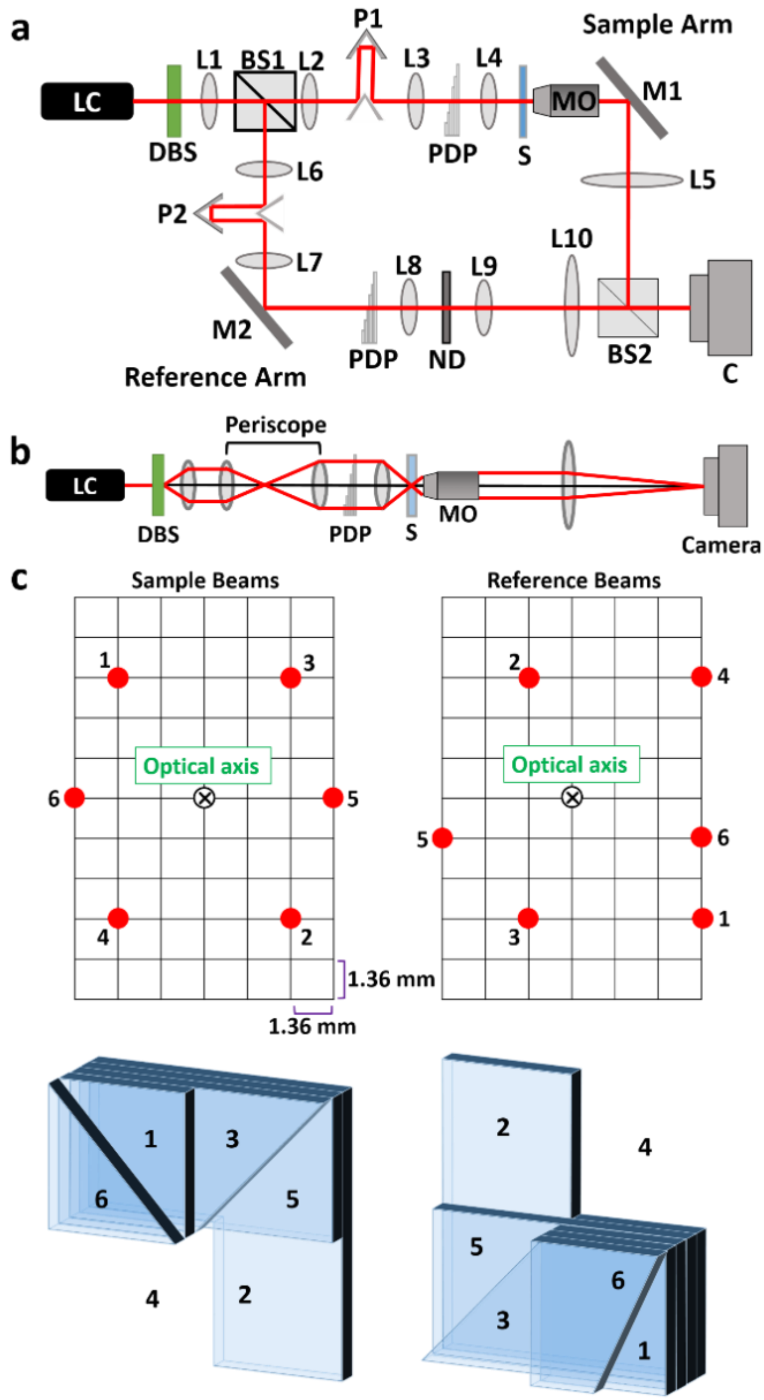

Fig. 2. Realization of 6PH using a modified Mach-Zehnder interferometer. (a) 6PH system for SA super-resolution. LC, low-coherence supercontinuum laser source; DBS, diffractive beam shaper; L1 – L10, lenses; BS1, BS2, beam splitters; P1, P2, periscopes; PDP, phase delay plate; S, sample; MO, microscope objective; M1, M2, mirrors; ND, neutral density filter; C, camera. The red line displays the optical axis and not the six sample and six reference beam paths. (b) Illustration of beam paths in sample arm for two sample beams at opposing angles from the optical axis. The region marked 'Periscope' is the location of periscope P1 in (a). (c) Top: Diagram of the beams used as the reference and sample beams and their positions relative to the optical axis immediately before the phase delay plates. Each vertex in the image corresponds to one of the 77 beams produced by the DBS in both arms. Only the numbered beams (red circles) are not blocked. Bottom: The corresponding sample and reference PDP structures.

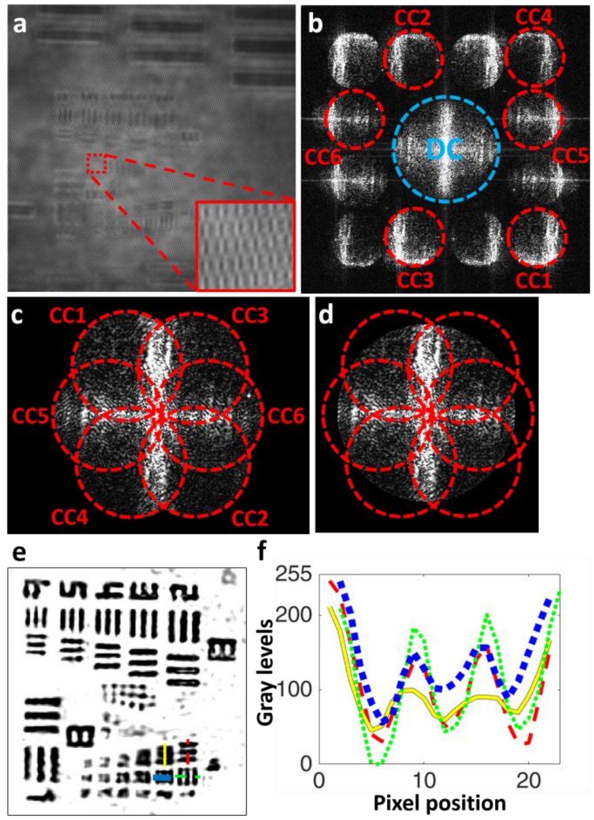

Fig. 3. SA super-resolution imaging based on 6PH. (a) Six-pack multiplexed hologram of a USAF target, experimentally acquired in a single camera exposure. Inset shows fringes magnified five times. (b) The corresponding spatial frequency power spectrum, after subtracting background image power spectrum. (c) Positioning of CC terms in the SA. CC numbering corresponds to matching sample beam from Fig. 2(c). (d) Same SA as in (c) after cropping to the largest possible circle, which makes the final image resolution isotropic. (e) Amplitude image produced from (d). (f) Profiles along the lines marked in e demonstrating the smallest resolvable elements.

The visibilities of the USAF elements from the standard off-axis holography amplitude image were calculated based on the profiles in Fig. 4(a). The vertical visibility of element 2 from group 8 was found to be 67%, while the horizontal visibility of the same element was calculated to be 70%. The same calculations were done for the vertical and horizontal profiles of element 3 from group 8 and the visibilities were found to be 30% and 42%, respectively. Thus, the corresponding resolution limit of the standard amplitude image is between 1.55 – 1.74 μm.

Following this, the visibilities of the USAF elements from the six-pack SA amplitude image were calculated based on the profiles in Fig. 3(f). The vertical visibility of element 1 from group 9 was found to be 61%, while the horizontal visibility of the same element was calculated to be 73%. The same calculations for the vertical and horizontal profiles of element 2 from group 9 determined that the visibilities were 24% and 30%, respectively. Thus element 1, possessing a line width of 0.98 μm, is the resolution cutoff for the six-pack SA.

Based on these results, the approximate increase in resolution is between 1.58 – 1.78 times the original resolution, corresponding to NAs of 0.395 – 0.445. This closely matches the expected increase in resolution which, based on the relative size and positions of the CC terms when constructing the SA, and after cropping the SA to a circle with no missing frequencies as illustrated in Fig. 3(d), was calculated to be 1.62 times.

For comparison, we also implement two-pack holography (2PH) and four-pack holography (4PH) by selecting only the frequencies covered by two terms, CC5 and CC6 from Fig. 3(c), and four terms, CC1

– CC4 from Fig. 3(c), respectively. The results and corresponding profiles are shown in Figs. 4(b) and 4(c), and the resolution limits for all amplitude images, including those of the six-pack SA and standard off-axis images, are shown in Fig. 5. In Fig. 4(b), one can see that the two CC term (2PH) amplitude image can resolve up to element 1 of group 9 in the horizontal direction, but only up to element 2 of group 7 in the vertical direction due to CC 5 and 6 having a very limited coverage of vertical frequencies. A similar limitation is seen in Fig. 4(c) where the four CC term (4PH) amplitude image can resolve up to element 1 of group 9 in the vertical direction, but only up to element 5 of group 8 in the horizontal direction due to the limited horizontal frequency coverage of CCs 1 – 4. Only by combining all six CC terms can we achieve the highest possible resolutions in all directions.

The main advantage of six-pack multiplexing for superresolution is that it enables the creation of a larger SA from dynamic acquisition as the six channels are acquired in a single exposure. Visualization 1 demonstrates the reconstructed amplitude image video of a dynamic USAF test target, translating laterally over time. The video was acquired at a rate of 22 frames per second.

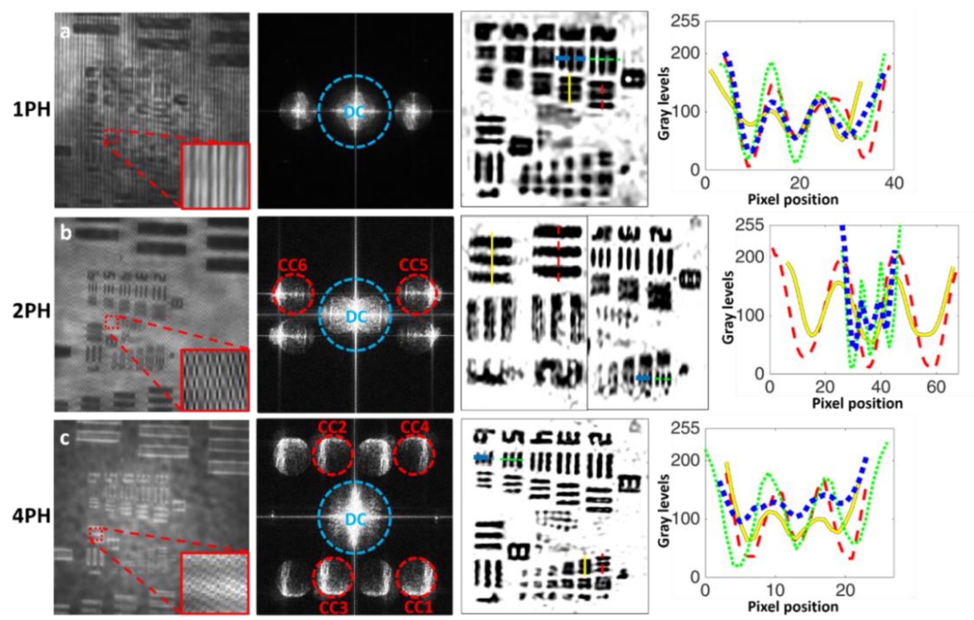

Fig. 4. Experimental results from 1PH, 4PH, and 6PH. (a) Standard off-axis hologram (1PH). (b) Two-pack hologram (2PH). (c) Four-pack hologram (4PH). From left to right column: hologram with inset showing fringes magnified five times, corresponding spatial frequency power spectrum, reconstructed amplitude image, and profiles at the locations marked on the amplitude image. For comparison, the 6PH results are shown in Fig. 3. For 2PH amplitude image: Left side shows elements from group 7. All other amplitude images show elements from groups 8 and 9.

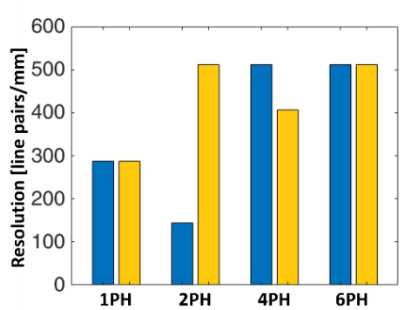

Fig. 5. Resolution limits in Figs. 3 and 4. For each group: first bar from the left is vertical resolution, second bar is horizontal resolution.

To further demonstrate the benefits of the proposed six-pack SA technique for dynamic samples, we obtained quantitative phase videos of flowing red blood cells, as well as flowing polymer beads, 1 μm in diameter. SAs were then produced for each video frame. The amplitude images and reconstructed optical path delay (OPD) profiles are shown in Fig. 6. In Figs. 6(a) and 6(b), we show SA amplitude images of a multi-layer sample of red blood cells from a single video frame using 1PH and 6PH, respectively. One can see that the resolution correspondingly increases when using 6PH as occurred with the images of the USAF target. We then produced OPD maps of Figs. 6(a) and 6(b), as shown in Figs. 6(c) and 6(d). As can be seen, not only does the 6PH SA improve the resolution of amplitude images, it produces the same effect in the OPD optical path delay (OPD) maps.

The resolution enhancement in the OPD profile is more clearly seen in the 1 μm bead reconstruction shown in Figs. 6(e)–6(g), with e and f displaying 1PH and 6PH OPD maps of microbeads. In Fig. 6(g), we can see the cross-section graph along one of the beads in 1PH and 6PH, demonstrating again that 6PH yields an improved resolution represented by a more localized peak of the corresponding graph.

Dynamic results of flowing red blood cells, including numerical refocusing using Fresnel propagation, are shown in Visualization 2, and dynamic results of flowing beads are shown in Visualization 3. Details on refocusing can be found in Appendix 1.

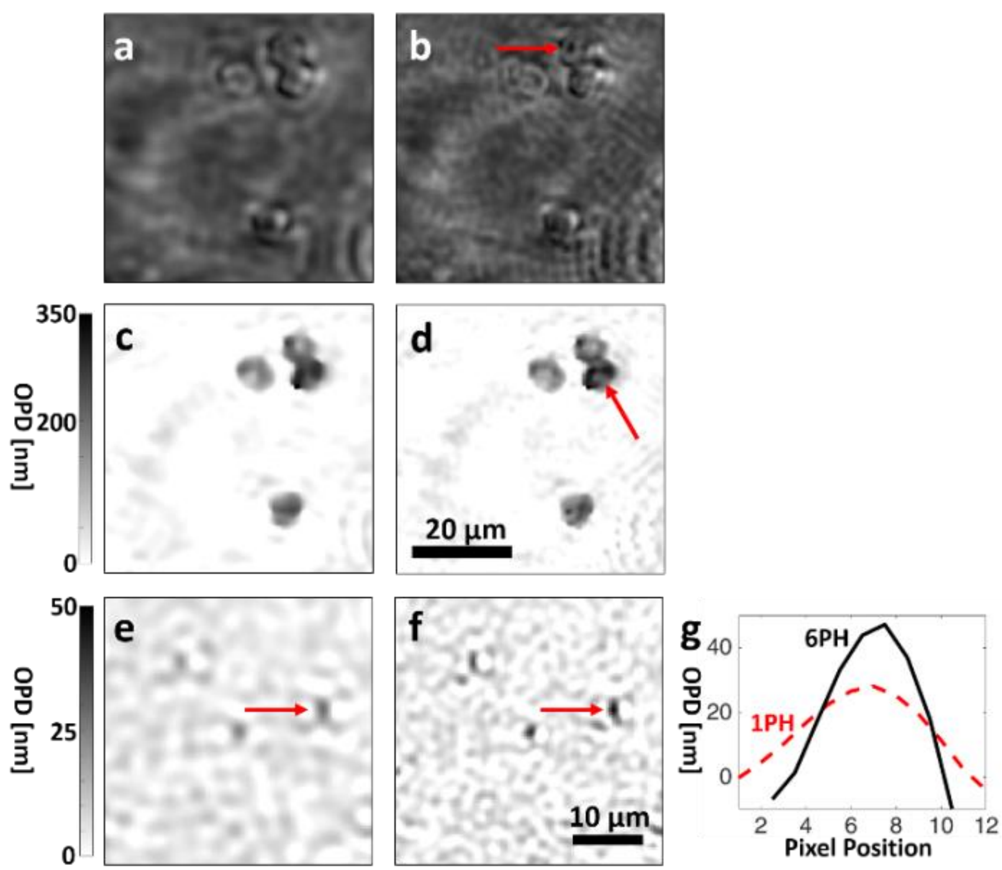

Fig. 6. Red blood cells and microbeads amplitude and quantitative phase (OPD) maps. (a,b) Amplitude images of a sample containing multi-layers of red blood cells using 1PH (a) and 6PH (b). (c,d) OPD maps corresponding to (a) and (b). Red arrows indicate resolution enhancement: indentations at the centers of red blood cells are now more visible. The color bar to the left of (c) applies to (c) and (d). (e), (f), OPD map of microbeads using 1PH (e) and 6PH (f). (g) Profiles of the bead in e and f indicated by the red arrows.

We used a simple 8-bit digital camera (DCC1545M, Thorlabs) and demonstrated both amplitude and phase imaging. As the six channels share the same dynamic range of the grayscale level of the camera, we experimentally quantified the signal to noise ratio (SNR) of a standard hologram reconstruction in comparison to six-channel SA reconstruction. This was done by calculating the mean value and standard deviation for the same rectangular region of the image in which no sample was present. The approximate SNR values were then defined as the mean value divided by the standard deviation. The SNR for the standard image was 19.2 while the SNR for the 6PH SA image was 13.3. This would indicate that the SNR has decreased by 41%. In order to compare the effect of shot noise on the SNR of each channel, we used Eq. (8) from [33], which predicted a decrease of at least 59% when comparing one channel to six channels. To test this predicted SNR decrease, we generated single-CC-term amplitude images from CCs 5 and 6, the only terms containing the lowest sample frequencies, and calculated the mean SNR of these images. The resulting SNR value was 7.5, indicating a 61% decrease in the SNR of a single channel of the six-pack hologram when compared to the standard hologram. This value closely matches the expected theoretical decrease in SNR of 59%. In any case, as shown in our results, our SNR decrease due to dynamic range sharing of only 256 grayscale levels is acceptable for the samples used even though some of the samples are not sparse, and both amplitude and phase reconstructions have been demonstrated. SNR decrease might be more significant for samples with higher absorbance, where cameras with higher bit-depth may have to be used. We have thoroughly quantified the SNR decrease for off-axis holographic multiplexing in [11].

5. Conclusion

We successfully implemented the first system capable of generating dynamic 6PH. The resulting multiplexed hologram was comprised of six off-axis holograms, each produced by illuminating the sample from a different angle, yet still utilizing the same number of camera pixels.

As shown, 6PH has the significant novelty of being more spatial bandwidth efficient than any other off-axis holographic configuration and even on-axis holography. This constitutes a change in the fundamental paradigm of holographic imaging. Furthermore, since the six channels are acquired at once, 6PH does not suffer from pixel registration problems, making it suitable for acquiring complex wavefronts of highly dynamic samples.

Although we have shown the first experimental realization of 6PH for SA superresolution imaging, this first 6PH realization sets the foundations for many other spatial hologram multiplexing applications reaching beyond the scope of the current paper. Various types of data can benefit from adaptions of the current system, enabling the acquisition of six parallel imaging channels while using the same number of camera pixels. These include field of view multiplexing, wavelength multiplexing, phase and fluorescence multiplexing, z-plane multiplexing, angular-illumination multiplexing, polarization state multiplexing, and many others. Thus, 6PH is expected to impact many fields involving rapid holographic wavefront acquisition.

Appendix 1

The precise details of the 6PH optical system described in brief in the manuscript and illustrated in Fig. 2(a) are as follows. Low-coherence laser light LC with a wavelength of 632.8 nm is emitted by a supercontinuum laser source (NKT SuperK EXTREME), followed by an acousto-optical filter (NKT SuperK SELECT) and a laserline filter (central wavelength: 632.8 nm, full width at half maximum: 3 nm). This low-coherence laser beam illuminates a diffractive beam shaper, DBS (DigitalOptics Corporation), producing 77 collimated beams in a diverging rectangular 11 x 7 pattern. The beams proceed to pass through biconvex lens L1 (50 mm focal length) and enter a 50:50 beam splitter, BS1. In the sample arm, the beams then pass through achromatic lens L2 (50 mm focal length) and enter periscope P1.

The purpose of lenses L1 and L2 is to pass the beams through the beam splitter while maintaining a 4f configuration with no magnification. The beams are essentially unchanged when passing periscope P1 and then enter achromatic lens L3 (150 mm focal length), where they are made parallel. Due to the ratio of the focal lengths of L2 and L3, the size of the pattern is magnified three times. This magnification creates a larger separation between the beams, increasing the angles at which the beams illuminate the sample after passing through lens L4, and making it easier to block all but the six desired beams illustrated in Fig. 2(c). Before passing through plano-convex lens L4 (35 mm focal length), the undesired beams are blocked and the remaining six beams pass through a phase delay plate PDP (shown in Fig. 2(c)), composed of 2 mm thick sections of glass that are glued together at the edges in order to prevent the glue from increasing the phase delays. This PDP induces a minimum optical path delay of 1.16 mm between the beams which, as the coherence length of the laser is 42.4 μm, prevents the six sample beams from interfering with each other. The six delayed sample beams then pass through L4, with beams 1 to 4 illuminating the sample S at an angle of 7.96° from the optical axis, and beams 5 and 6 illuminating the sample at an angle of 6.64° from the optical axis. By illuminating the sample at the described angles, beams 1 to 4 downshift the sample frequencies by a factor of 55.0% of the NA of the microscope objective MO (Leica 439, 10× magnification, 0.25 NA, infinity corrected), and beams 5 and 6 downshift the sample frequencies by a factor of 45.8% of the numerical aperture of the microscope objective. The light scattered by the sample is then collected and imaged on digital camera C (DCC1545M, Thorlabs, 8-bit monochromatic CMOS, 1280 × 1024 square pixels of 5.2 μm each) by the microscope objective and achromatic tube lens L5 (300 mm focal length), passing through the 50:50 beam splitter BS2 on the way, with the final image magnification being 16.33, and the diffraction limited spot size being 2.53 μm.

In the reference arm, the beams pass through lens L6, periscope P2, and lens L7, which are identical to L2, P1, and L3, respectively. Periscopes P1 and P2 are each composed of two stationary mirrors placed along the optical axis with an angle of 270° between their reflective faces, and a retroreflector composed of two mirrors with an angle of 90° between their reflective faces. The retroreflector in P2 is mounted on a translation stage that can be used to carefully adjust the distance between the retroreflector and the two stationary mirrors. This enables us to adjust the optical path length of the reference arm in order to compensate for the delay induced by the sample. After passing through L7, all but the requisite six beams are blocked, as illustrated in Fig. 2(c), and the beams pass through the PDP illustrated in this figure, which is similar to the plate in the sample arm but with the glass segments arranged differently in order to correspond to the different beam pattern. The pattern of the six reference beams differs from the pattern of the six sample beams as it is designed to generate off-axis angles suitable for multiplexing six holograms, and the PDP of the reference arm is designed to match the phase delays between the six matching sample and reference beam pairs. The reference beams then pass through achromatic lenses L8 (75 mm focal length), L9 (100 mm focal length), and L10 (150 mm focal length), with reference beams 2, 3, 5, and 6 illuminating the camera at an off-axis angle of 2.45°, and beams 1 and 4 illuminating the camera at an off-axis angle of 2.32°.

While all lenses in the sample arm, including L1 and L2, are arranged in a 4f configuration, the distances between L8 and L9, as well as L10 and the camera, are not 4f but rather 155 mm and 200 mm, respectively. This is necessary in order to create high off-axis angles while having all six reference beams illuminate the same point on the camera. The geometry utilized to generate these off-axis angles leads to an estimated 33% decrease in reference beam diameter. To compensate for the corresponding increase in intensity, a neutral density filter, ND, of optical density 1.5, was placed after lens L8.

After constructing the system, a 6PH image of a USAF target was captured and used to determine CC term positioning in the SA. Initial rough alignment was done by positioning the six CC terms based on the known power spectrum pattern (cross shape) produced by the USAF. Fine tuning of the alignment was achieved empirically by individually shifting the locations of opposing pairs of CC terms, in 1 pixel increments, then adding the two terms together to create a 2-term SA while taking the average value of overlapping pixels, and then examining the resulting amplitude image and comparing it to the known USAF design. It was easy to tell when the CC terms were even slightly out of alignment, as we could see that the three lines in at least one of the elements of the USAF target would either become four lines (when the CC terms were too far apart) or a blurred approximation of two lines (when the CC terms were too close). This determination of CC term position only needs to be performed once. After this process, stitching of the SA was done by using only the frequencies of the

CC term with the highest maximum power where two or more CC terms overlap. Once the six-pack hologram is captured and the SA is constructed, numerical refocusing of the SA image is possible.

In our implementation, the reconstruction produced a SA that increased the resolution of the image by a factor of approximately 1.62. Further resolution increase is possible with this system, with an estimated maximum increase in resolution of 1.66 if the lens before the sample possesses a non-standard focal length of 32.5 mm. A lens of focal length smaller than 32.5 mm would downshift the sample frequencies too much and would cause us to miss some of the lowest frequencies. The phase delay plates used in this work are hand-made, and had air gaps between the 2 mm glass slides comprising each step which led to undesired reflections and decreases in beam intensity. Additional improvements to the system can be made by using phase delay plates of solid glass with no air gaps. In addition, a diffractive beam shaper that only outputs the desired beams could be used, allowing us to save up to 87% of the laser intensity, rather than outputting a 2D array containing 77 beams and blocking the unwanted beams. Finally, to effectively decouple the correlation between illumination angle and beam diameter that is present in the system, it would be necessary to place 4f systems of microlenses, so that beams would travel in parallel.

In this paper, we used a filtered supercontinuum source to achieve controlled coherence length. Other collimated light sources that possess a similar coherence length, such as a laser diode, could be used. However, any decrease in the coherence length will decrease the area upon which we see interference on the camera, while increasing the coherence length can lead to cross-talk between the beams, which can be solved by increasing the thickness of the PDP.

Funding

H2020 European Research Council (ERC) (678316)

Acknowledgments.

We thank Dr. Itay Barnea for preparing the red blood cell samples.

References

1. I. Yamaguchi and T. Zhang, "Phase-shifting digital holography," Opt. Lett. **22**(16), 1268-1270 (1997).
2. E. Cuche, F. Bevilacqua, and C. Depeursinge, "Digital holography for quantitative phase-contrast imaging," Opt. Lett. **24**(5), 291-293 (1999).
3. P. Girshovitz, I. Frenklach, and N. T. Shaked, "Broadband quantitative phase microscopy with extended field of view using off-axis interferometric multiplexing," J. Biomed. Opt. **20**(11), 111217:1-6 (2015).
4. N. Turko, P. Eravuchira, I. Barnea, and N. T. Shaked, "Simultaneous three-wavelength unwrapping using external digital holographic multiplexing module," Opt. Lett. **43**(9), 1943-1946 (2018).
5. W. Koek, N. Bhattacharya, J. J. M. Braat, V. Chan, and J. Westerweel, "Holographic simultaneous readout polarization multiplexing based on photoinduced anisotropy in bacteriorhodopsin," Opt. Lett. **29**(1), 101-103 (2004).
6. Y. Nygate, G. Singh, N. Turko, and N. T. Shaked, N.T. "Simultaneous off-axis multiplexed holography and regular fluorescence microscopy of biological cells," Opt. Lett. **43**(1), 2587-437 (2018).
7. D. Jin, R. Zhou, Z. Yaqoob, and P. T. C. So, "Dynamic spatial filtering using a digital micromirror device for high-speed optical diffraction tomography," Opt. Express **26**(1), 428-437 (2018).
8. L. Wolbromsky, N. Turko, and N. T. Shaked, "Single-exposure full-field multi-depth imaging using low-coherence holographic multiplexing," Opt. Lett. **43**(9), 2046-2049 (2018).
9. Z. Liu, M. Centurion, G. Panotopoulos, J. Hong, and D. Psaltis, "Holographic recording of fast events on a CCD camera," Opt. Lett. **27**(1), 22-24 (2002).
10. M. Rubin, G. Dardikman, S. K. Mirsky, N. Turko, and N. T. Shaked, "Six-pack off-axis holography," Opt. Lett. **42**(22), 4611-4614 (2017).
11. G. Dardikman, N. A. Turko, N. Nativ, S. K. Mirsky, and N. T. Shaked, "Optimal spatial bandwidth capacity in multiplexed off-axis holography for rapid quantitative phase reconstruction and visualization," Opt. Express **25**(26), 33400-33415 (2017).
12. J. Picazo-Bueno and V. Mico, "Opposed-view spatially multiplexed interferometric microscopy," J. Opt. **21**(3), 035701 (2019).
13. X. Lai, C. Cheng, Y. Lin, and H. Tu, "Angular-polarization multiplexing with spatial light modulators for resolution enhancement in digital holographic microscopy," J. Opt. **19**(5), 055607 (2017).

14. L. Huang, H. Mühlenbernd, Y. Wang, and T. Zentgraf, "Metasurface holography with multiple channels," Progress in Electromagnetic Research Symposium (PIERS), Shanghai (2016).
15. J. Picazo-Bueno, Z. Zalevsky, J. García, and V. Micó, "Superresolved spatially multiplexed interferometric microscopy," Opt. Lett. **42**(5), 927-930 (2017).
16. T. Tahara, R. Otani, K. Omae, T. Gotohda, Y. Arai, and Y. Takaki, "Multiwavelength digital holography with wavelength-multiplexed holograms and arbitrary symmetric phase shifts," Opt. Express **25**(10), 11157-11172 (2017).
17. P. Zdańkowski, V. Mico, J. Picazo-Bueno, K. Patorski, and M. Trusiak, "Multi-beam spatially multiplexed interference microscopy for phase objects examination," SPIE Optical Engineering and Applications, San Diego (2018).
18. J. Picazo-Bueno, Z. Zalevsky, J. García, C. Ferreira, and V. Micó, "Spatially multiplexed interferometric microscopy with partially coherent illumination," J. Biomed. Opt. **21**(10), 106007 (2016).
19. J. Picazo-Bueno, M. Trusiak, J. García, K. Patorski, and V. Micó, "Hilbert–Huang single-shot spatially multiplexed interferometric microscopy," Opt. Lett. **43**(5), 1007-1010 (2018).
20. Y. Lin, H. Chen, H. Tu, C. Liu, and C. Cheng, "Optically driven full-angle sample rotation for tomographic imaging in digital holographic microscopy," Opt. Lett. **42**(7), 1321-1324 (2017).
21. X. Lai, H. Tu, Y. Lin, and C. Cheng, "Coded aperture structured illumination digital holographic microscopy for superresolution imaging," Opt. Lett. **43**(5), 1143-1146 (2018).
22. Y. C. Lin, H. Y. Tu, X. R. Wu, X. J. Lai, and C. J. Cheng, "One-shot synthetic aperture digital holographic microscopy with non-coplanar angular-multiplexing and coherence gating," Opt. Express **26**(10), 12620-12631 (2018).
23. M. Paturzo, P. Memmolo, L. Miccio, A. Finizio, P. Ferraro, A. Tulino, and B. Javidi, "Numerical multiplexing and demultiplexing of digital holographic information for remote reconstruction in amplitude and phase," Opt. Lett. **33**(22), 2629-2631 (2008).
24. J. Massig, "Digital off-axis holography with a synthetic aperture," Opt. Lett. **27**(24), 2179-2181 (2002).
25. T. Kreis, M. Adams, and W. Jueptner, "Aperture synthesis in digital holography," International Symposium on Optical Science and Technology, Seattle, WA, United States (2002).
26. V. Mico, Z. Zalevsky, P. García-Martínez, and J. García, "Synthetic aperture superresolution with multiple off-axis holograms," J. Opt. Soc. Am. A **23**(12), 3162-3170 (2006).
27. L. Granero, V. Micó, Z. Zalevsky, and J. García, "Synthetic aperture superresolved microscopy in digital lensless Fourier holography by time and angular multiplexing of the object information," Appl. Opt. **49**(5), 845-857 (2010).
28. V. Mico, Z. Zalevsky, and J. Garcia, "Synthetic aperture microscopy using off-axis illumination and polarization coding," Opt. Comm. **276**(2), 209-217 (2007).
29. C. Yuan, H. Zhai, and H. Liu, "Angular multiplexing in pulsed digital holography for aperture synthesis," Opt. Lett. **33**(20), 2356-2358 (2008).
30. L. Martínez-León and B. Javidi, "Synthetic aperture single-exposure on-axis digital holography," Opt. Express **16**(1), 161-169 (2008).
31. V. Micó, Z. Zalevsky, C. Ferreira, and J. García, "Superresolution digital holographic microscopy for three-dimensional samples," Opt. Express **16**(23), 19260-19270 (2008).
32. A. Calabuig, V. Micó, J. Garcia, Z. Zalevsky, and C. Ferreira, "Single-exposure super-resolved interferometric microscopy by red–green–blue multiplexing," Opt. Lett. **36**(6), 885-887 (2011).
33. F. Charrière, T. Colomb, F. Montfort, E. Cuche, P. Marquet, and C. Depeursinge, "Shot-noise influence on the reconstructed phase image signal-to-noise ratio in digital holographic microscopy," Appl. Opt. **45**(29), 7667-7673 (2006).